

An Interpretable Prediction Model for Obesity Prediction using EHR Data*

Mehak Gupta^{1,†}, Thao-Ly T. Phan^{3,4}, George Datto^{3,4}, Timothy Bunnell^{1,2}, Rahmatollah Beheshti^{1,5,†}

¹ Computer and Information Sciences, University of Delaware, Newark, DE, USA

² Department of Biomedical Research, Nemours Alfred I. duPont Hospital for Children, Wilmington, DE, USA

³ Department of Pediatrics, Nemours Alfred I. duPont Hospital for Children, Wilmington, DE, USA

⁴ Department of Pediatrics, Thomas Jefferson University, Philadelphia, PA, USA

⁵ Epidemiology Program, University of Delaware, Newark, DE, USA

† Email: mehakg@udel.edu (MG), rbi@udel.edu (RB)

ABSTRACT

Childhood obesity is a major public health challenge. Obesity in early childhood and adolescence can lead to obesity and other health problems in adulthood. Early prediction and identification of the children at a high-risk of developing childhood obesity may help in engaging earlier and more effective interventions to prevent and manage this and other related health conditions. Existing predictive tools designed for childhood obesity primarily rely on traditional regression-type methods without exploiting longitudinal patterns of children's data (ignoring data temporality). In this present, we present a machine learning model specifically designed for predicting future obesity patterns from generally available items on children's medical history. To do this, we have used a large unaugmented EHR (Electronic Health Record) dataset from a major pediatric health system in the US. We adopt a general LSTM (long short-term memory) network architecture for our model for training over dynamic (sequential) EHR data. We then modified and extended the architecture to accept static (demographic) data related to each individual. We have additionally included a set embedding and attention layers to compute the attention scores of each hidden layer corresponding to each input timestep. The attention score for each timestep were computed as an average score given to all the features associated with the timestep. These attention scores added interpretability at both timestep-level and the features associated with the timesteps.

CCS CONCEPTS

• Computing methodologies • Machine learning • Machine learning approaches • Neural networks

KEYWORDS

• Childhood obesity • Electronic health records • Temporal data • Deep learning • Long short-term memory • Transfer learning

1 Introduction

Childhood obesity is a major public health problem across the globe as well as in the US. In 2019, the prevalence of obesity was 18.5% affecting almost 13.7 million US children and adolescents aged 18 or less [1]. Childhood obesity can continue into adulthood and is known to be a major risk factors for chronic diseases such as diabetes, cancer, and cardiovascular diseases [2]. Preventing childhood obesity has been actively pursued in pediatric programs. However, decades of rigorous research and experiments have shown that prevention and management of obesity is not easy [3]. This is partly due to our limited understating of obesity and the complex interactions among myriad of various factors, including biological and environmental ones, that are known to contribute to obesity. Additionally, knowing the limited resources available to the healthcare systems, identifying children at the highest risk of developing obesity is another obstacle facing prevention programs. In such a complex domain, predictive models have been shown to be effective in informing decision makers and providers in designing and delivering more effective interventions.

In this study, we created a predictive model of childhood obesity using a longitudinal dataset of children derived from the electronic health records (EHR) of a pediatric healthcare system. EHR data consists of clinical data along with its related temporal information. EHR datasets are generally very sparse and complex due to the large amount of information captured and irregular sampling. EHR relate to the records of patients' visits, which consist of conditions diagnosed, drugs prescribed, procedures performed, and laboratory results recorded in any visit. The number of unique condition diagnosis, drugs, procedures, and lab results collected in EHR datasets is generally huge. This leads to a very large feature (input) space for a prediction model, despite each visit having only a very small subset of total unique conditions, drugs, procedures and measurements recorded. Due to the sparse feature space associated with each visit, we removed features which are absent or not recorded in more than 98% of the population.

We present a set of predictive models that consider the temporal changes of the children's health patterns. A large body of research has shown that childhood obesity patterns are sensitive to different patterns of weight gain such that more acute and rapid weight gain predicts a different severity of obesity than more chronic and gradual weight gain [4]. Traditional approaches that have been used in this domain rely on aggregated data, which ignores the temporality of data. We used a Recurrent Neural Network (RNN) architecture with Long Short-term Memory (LSTM) cells, which learns the patient representation from the temporal data collected over various visits of the patient. This patient representation captures the temporality of input EHR data. Additionally, as one of the major drawbacks of deep learning models like RNNs is the lack of interpretability, we have used embedding weights on the input layer and softmax activations on LSTM layers to calculate the importance of the features and attention weights for each input timestep. The importance score for the features and attention weights for timesteps were visualized to determine important features and timesteps at the individual and population level. Apart from the time series data collected for visits of patients over time, EHR data also contains static data. The static data in EHR data does not change with every visit. This data consists of sex, race, ethnicity and zip code for each patient. We used separate feed-forward network for the static data and concatenated the output from this feed-forward network to the outputs obtained from LSTM cells.

Our models can predict the body mass index (BMI defined as height in kg over height squared in meter) in various ages. Having the estimated BMI values, we specifically look at the problem of classifying children as obese (above 95th percentile), and non-obese at the ages between 3 and 20 years according to the growth charts for children and teens provided by US Center for Disease Control (CDC) [5]. As the model predicts the BMI values fairly, it can be used for answering similar types of questions other than what is the focus of the current study. This specific problem (classifying obese versus non-obese) relates to identifying those at the highest risk. Compared to existing obesity predictive models in this domain, our model uses a much larger dataset (44 million rows with 68029 unique patients) for training and considers a larger set of confounders for predicting outcomes. Unlike existing models that focus at single age point in childhood and adolescence [6], we created different prediction models for different input and outputs ages. Also, our model is based only

on the EHR data already available in the hospitals. Some work used questionnaires [7], and census data to predict obesity [8]. We did not use any other external data, and as the features that we use are commonly recorded in any standard EHR system, our models can be readily applicable to many healthcare systems. This also means that our models can be used with no additional cost in collecting any external data.

The main contributions of this paper include presenting a prediction model which uses LSTM cell layers on multivariate irregularly spaced time series data to predict outcomes at 3 different time points in future, and proposed a mechanism to add interpretability to this model. Our mechanism adds interpretability at both feature-level and timestep-level for the predictive task by computing embedding weights on input layer and timestep attention weights on the LSTM layer. This provides insights into important clinical events at individual and population level. In our experiments, we perform comparisons between machine learning techniques that ignore temporality with the machine learning models that capture temporality in the data (including our models) in predicting childhood obesity, and show that our models can achieve significantly better results.

2 Related Work

Clinical predictive models are becoming more and more prevalent [9]. Until recently most of the clinical predictive models were primarily developed based on regression and logistic regression or other types of statistical analysis [6]. Over the last decade, there has been an increase in the medical data collected in the form of EHR. To use the traditional methods, input features need to be selected by medical domain experts. Traditional methods (including the machine learning ones) are not very effective in capturing the non-linear and temporal relationships in the complex EHR data. Recently, deep learning techniques have shown a lot of success in clinical predictive modeling [10].

Many of deep learning studies in this domain use RNNs, which refer to a special set of deep neural architectures used on sequential datasets. RNNs take advantage of the concept of parameter sharing across the model. Unlike the basic feedforward network where each input feature is learned separately and have separate parameters, RNNs share the parameters and generalize the model across different forms on input. This property of RNN is used for many natural language processing (NLP) problems where the same information can be found in different locations depending on the formation of input data. For temporal data RNNs can be also used to learn long-term dependencies by sharing parameters through the deep computational graphs. However, remembering long-term dependencies using RNNs generally faces the vanishing gradient problem (gradient values becoming too small). Two common ways to approach this problem are using LSTM cells and Gated Recurrent Unit (GRU) cells. In this paper, we are using LSTM cells. Hochreiter et al. [11] introduced the gating mechanism where the gradient can flow for long durations. These gates learn to keep important information and throw irrelevant information from previous time steps. This way, they pass on the important information in the network for long durations.

Many clinical predictive models have been developed using RNN and LSTMs to predict various health problems like heart failure [12] [13] [14], diabetes [15], high blood pressure [16], and hospital readmission [17]. However, and despite the urgent need, there is not a lot of work done in the field of obesity predictive modeling leveraging large scale datasets and advanced machine learning techniques. Most of existing work rely on traditional machine learning methods. Example studies include using logistic regression [18] [19] [20] [21], linear regression [22], and the random forest [8]. Our study used deep learning technique to capture the temporal nature of the data. The major limitation of existing obesity models is twofold. First, available obesity models focus on single (or only a few) future point prediction. For instance, several models have been developed for predicting obesity at the age of 5 [4]. These single-point prediction models cannot be generalized to predict the future BMI trajectories starting from various points in early childhood and adolescence. Obesity is prevalent in all age groups in childhood and adolescence. This makes the application of these models limited, as they cannot assist in predicting obesity status in other ages. Second, using aggregated patterns instead of longitudinal patterns for developing the models. For obesity, this is a major limitation, since rigorous research has shown that longitudinal patterns of obesity-related indexes (such as

body-weight) have a very strong correlation with the future obesity patterns [12]. Aggregating EHR datasets (e.g., by calculating the average values) loses valuable knowledge from this type of time-series datasets. One of the major drawbacks of deep learning models is the lack of interpretability. The lack of interpretability reduces the value of prediction models especially in medical domain. If medical practitioners cannot understand how the outcome is predicted by a model, relying on the model’s outcomes will not be practical. Many attempts have been made recently to make sense of the outcome of these models. Bahdanau et al. [23] proposed the attention mechanism which is used in NLP for machine translation. This attention mechanism can improve the interpretability at time-level, i.e., it gives attention scores to timesteps. However, for multivariate time-series we also need to consider feature importance at each timestep. Zhang et al. [24] used hierarchical attention mechanism by using convolutional operation. Choi et al. [25] develop an interpretable model with two levels of attention weights learned from two reverse-time GRU models, respectively. In our work, we continue the use of attention mechanism to improve interpretability of the RNN based models for multivariate time-series to get importance score for timesteps and then get the importance score for each feature in the timesteps.

3 Data

3.1 Dataset description

The EHR data used in this work was extracted from the Nemours Children Health System, which is a large network of pediatric health in the US primarily spanning the states of Delaware, Pennsylvania, and New Jersey. The dataset is a portion of the larger PEDSnet dataset, containing EHR data from over 10 major US Children’s Health Systems [26]. Inclusion criteria for patients in our dataset included: (i) at least 5 years of medical history, (ii) no evidence of Type 1 diabetes, (iii) no evidence of cancer, sickle cell disease, developmental delay, or other complex medical conditions. An equal number of normal weight and overweight or obese patients were selected by random sampling from the normal weight population. The dataset was anonymized. Further details about the anonymization process are provided in Supplemental Materials. All of the dates were skewed randomly per patient by +/- 180 days. All the data access and processing steps were approved by Nemours Institutional Review Board. The final dataset consisted of 44,401,791 records from 68,029 distinct patients. Each record captures the timestamp for a visit start and end time and all the condition, procedure, drug, and measurement variables recorded for that visit. It also contains demographic data for each patient. The medical codes are standardized terminologies of SNOMED-CT, RxNorm, CPT, and LOINC [27] for both clinical and demographic facts. Some facts about the data are listed in Table 1.

Table 1: EHR Data Statistics

Name	Value
Total number of patients	68,029
Total number of visits	44,401,791
Avg. number of visits per patient	51
Number of females	31,014 (45%)
Number of Males	37,015 (54%)
Avg age of a patient	5
Race and Ethnicity	
White or Caucasian	33244
Black or African American	25329
Non-Hispanic or Latino	58894
Others	17834

3.2 Data Representation and Preprocessing

The EHR data extracted for this study consisted of 20,300 condition diagnosis variables, 10,167 procedure variables, 6,163 drug variables, and 7,693 lab-results (measurement) variables. All the condition and procedure variables were recorded as binary variables (1 if present and 0 if not recorded for the visit). Few drug variables were recorded as continuous variables where the values contain information about the amount of drug prescribed to a patient in a visit. However, many drug variables were recorded as binary variables and did not have the amount of drug prescribed information in the cohort. Measurement variables in the cohort were recorded as continuous variables. These continuous variables were normalized for model training.

EHR data consists of patient records as sequence of visits with each visit containing various medical codes. We represented EHR data using incremental representation where we first represent medical codes using code-level representation, then we use code-level representation of all medical codes for each visit record and represent visits using visit-level representation, and then we use visit-level representation for each visit of each patient and represent patients using patient-level representation. More details about these representations are provided in sections below.

3.2.1 Code-level Representation:

In code-level representation, medical codes consist of all the unique condition, drug, procedure and measurement variables in the complete data. We denote condition codes with the vector $C: \{c_1, c_2, \dots, c_{|C|}\}$ with a size of $|C|$, drug codes with the vector $D: \{d_1, d_2, \dots, d_{|D|}\}$ with a size of $|D|$, procedure codes with the vector $P: \{p_1, p_2, \dots, p_{|P|}\}$ with a size of $|P|$, and measurement codes $M: \{m_1, m_2, \dots, m_{|M|}\}$ with a size of $|M|$.

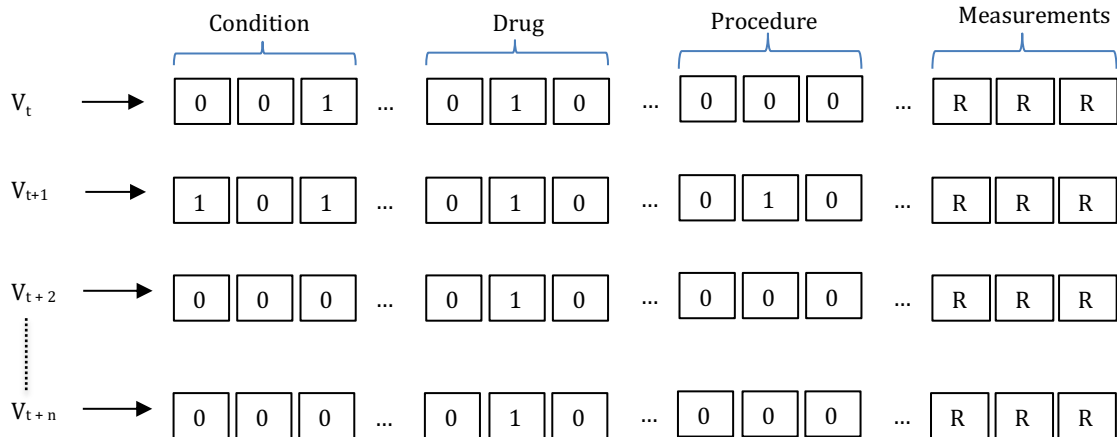
3.2.2 Visit-level Representation:

We denote visit at time t as V_t , which is the concatenation of condition, drug, procedure and measurement code vectors. The size of V_t is $|V|=|C| + |D| + |P| + |M|$. We represented condition, drug and procedure codes for visit V_t as binary vectors $C_t \in \{0,1\}^{|C|}$, $D_t \in \{0,1\}^{|D|}$, and $P_t \in \{0,1\}^{|P|}$ respectively where “1” represents the presence of the corresponding code for a visit V_t . All the measurement variables were represented by the corresponding continuous values $M_t \in \mathbb{R}^{|M|}$ for visit V_t . Fig. 1 depicts the visit-level representation of our EHR data. EHR data for each patient is the sequence of visit-level vectors for that patient.

3.2.3 Patient-level Representation:

Patient-level representation is sequence of visit vectors for the patient. We denote patients $S: \{s_1, s_2, \dots, s_{|M|}\}$ as S , where the i -th patient s_i with T visits is represented as matrix $s_i \in \mathbb{R}^{|T| \times |V|}$

Fig 1. Representation of EHR data. V_t represents the visit vector which consists of Condition, Drug, procedure and Measurement variables. Sequence of all visit vectors for a patient represents patient matrix.

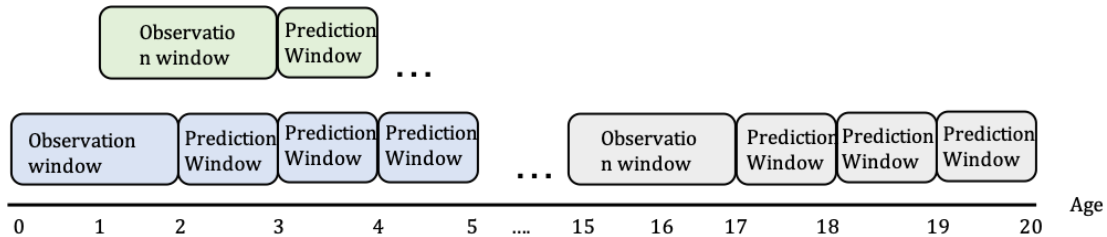


In addition to the medical data which changes with each visit, the EHR data also consists of static demographic data which does not change with every visit. Demographic information consists of sex, race, ethnicity and zip code (indicating the approximate location of the patient). We represented demographic variables i.e., sex, race, ethnicity and zip code as category variables. Table 1 shows the distribution of race and ethnicity distributions in the data. Insurance information is also represented as category variable.

The visit-level representation of complete EHR data consists of large number of features including all unique condition, drug, procedure, and measurement variables. Many of these features are not present in most of the population. We removed the features which do not have enough information and kept only the events that occurred in at least 2% of the population in the cohort to reduce the sparsity of the feature space. The feature space reduced to 3% of original when we only considered features that have enough information. Total number of features in final cohort were 1737.

We divided final data into sub-cohorts for different age ranges to predict obesity between 3 to 20 years of age. The data is extracted such that each patient has at least 5 years of data, and sub-cohorts for every 5-year of age range are created. Due to reasons like relocation and hospital change, a patient might not have data for all ages from 0 to 20 years. We divided the complete cohort into 5 years of age ranges starting from the ages between 0 to 15 years, which resulted in 16 age cohorts (0 to 5, 1 to 6, ..., 15 to 20). Picking more than 5 years of data would have resulted in small number of patients as there were fewer patients who have records of more than 5-year at one facility. For every 5-year data, we then used a fixed observation window of the initial 2-year, and predicted obesity for 1, 2 and 3 years in future. This way, we ended up with 48 sub-cohorts by creating 3 sub-cohorts for each of the 16 5-year time-periods. For each of the 48 models, we used only those samples with at least one visit in the observation and one visit in the prediction window. Fig. 2 depicts the way we created the sub cohorts and the observation window and shows the prediction window for these cohorts. Prediction models are trained on data in the observation window to predict the future BMI value in the respective prediction window.

Fig. 2 Sub cohort design and observation and prediction window for each sub-cohort. For each observation window there are 3 different prediction windows. As an example, shown below for observation window 0-2 years there there prediction windows 1 year which predicts at age of 3 years, 2 years which predicts at age of 4 years and 3 years which predicts at age of 5 years.



4 Method

Our proposed model is used to predict future BMI values, which are then used to classify patients as obese (more than 95th percentile) or non-obese (less than 95th percentile). The classification of BMI for different percentiles is done according to the BMI-for-age charts provided by US Centers for Disease Control and Prevention (CDC) [5]. CDC tables label children based on the age, gender and BMI for children from 24 months to 20 years of age. Children in the top 95 percentile are labeled as obese. For infants aged from 0 to 2 years, classification is performed according to the Data Table of Infant Weight-for-age Charts, also provided by CDC [28].

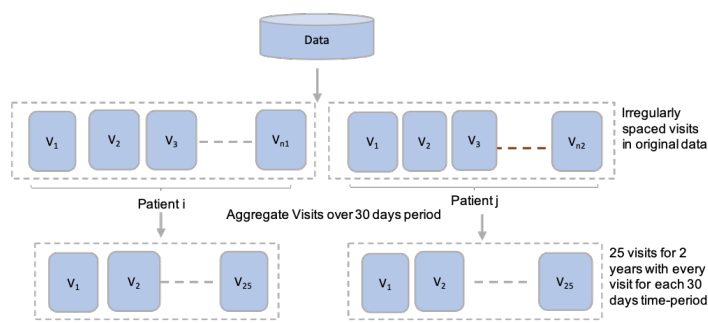
4.1 Baseline Model

As briefly discussed in the Related Work Section, comparable predictive models of childhood obesity are not being used in clinical settings for screening or consulting (including at Nemours Health System where the data comes from). Therefore, to evaluate the performance of our proposed LSTM-based model, we created two baseline models that follow the traditional methods and aggregate the dataset while ignoring the temporality of the EHR data. We used linear regression and random forest regressor as the baseline models for comparison. To do this, we aggregated data over all the visits for each patient corresponding to any of the input sub-cohorts. All the visit records in the observation window are aggregated for each patient. Target labels will be the labels at the prediction age. Aggregation for binary medical codes of condition, drug and procedure type is performed such that each medical code represents the frequency of its occurrence over the 2 years, and for continuous variables we took average over the 2 years. For the BMI and body weight, we took the maximum BMI and bodyweight recorded in the observation window. We also took the last BMI and body weight recorded for the observation window. BMI is classified as non-obese (less than 95th percentile), and obese (more than 95th percentile).

4.2 LSTM model

After obtaining all the sub-cohorts as explained in Section 3.2, we transformed the data so that it can be given as input to the LSTM model. Clinical visits obtained in Section 3.2 are represented by the medical codes associated with that visit. In general, (clinical) visits have irregular time intervals and each patient has a different number of visits. To transform these irregularly spaced and unequal number of clinical visits, we combined the visit data over a small fixed time window resulting in an equal number of time intervals. We combined visits over the 30-day time-periods for each observation window of the 2-year training windows, resulting in 25 equally spaced sequences for each patient. Fig. 3 shows how new sequences are obtained from unequal and irregularly spaced input time sequences. Any condition, drug and procedure variable observed at least once over 30-day time-period is denoted by 1 in new sequences. Continuous variables were averaged over the 30-day time-period. If there are no visits for a patient in any of the 30-day time-periods, the corresponding vector for that period contained all zeros. The zero vectors acted as padding to maintain equal sequence length for all patients. Such equally spaced time intervals between input time series are preferred representation for RNN models. In addition to conditions, procedure, drugs, and measurements the time intervals between each visit sequence were also added to the end of each visit's vectors. These time intervals capture the time intervals between the non-empty sequences. This procedure (adding time interval values) has been shown to enrich the time-series input in other similar studies [14].

Fig. 3 Time sequences for LSTM model – Irregularly spaced visits for each patient (such as patient i and j) in each 2 year period is mapped to 25 equally distributed intervals.

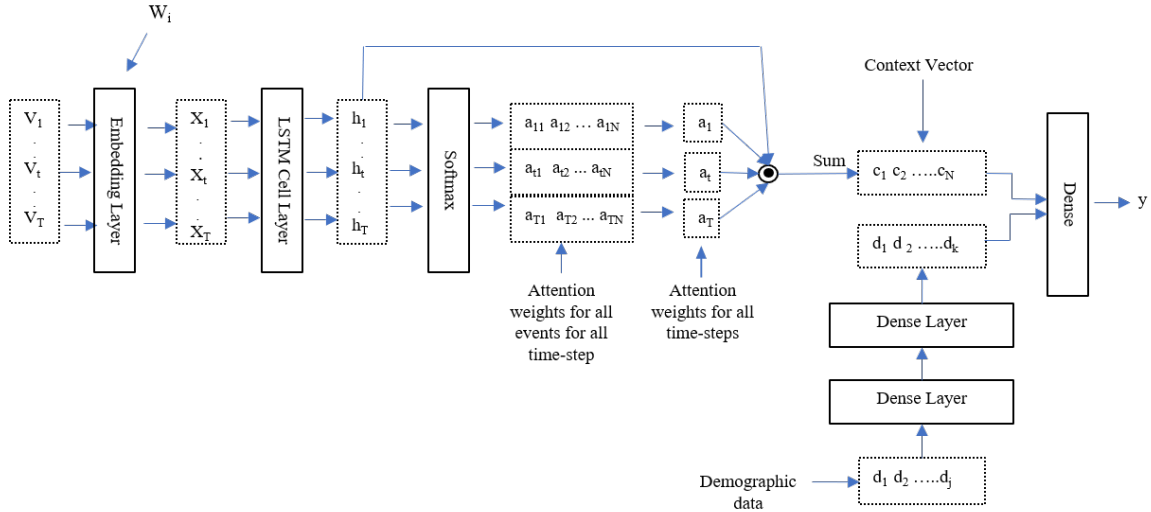


We used LSTM cells in the recurrent neural network for training our model over sequential visit-level (dynamic) data. The output of the LSTM layer was then concatenated with the set of demographics (static) data. This concatenated output is then passed through dense layers for predicting BMI value. The architecture of the complete model is shown in Fig. 4.

4.3 Interpretability

While deep learning models show superior performances compared to traditional machine learning models, they are difficult to interpret due to their so called “black box” architecture [29]. This may reduce the practicality of deploying them in medical domains. To mitigate such concerns, we enhanced our basic LSTM model to add some level of interpretability. Because of the mixed nature of our datasets, we have considered two levels of interpretability as time-level and feature-level interpretability. Time-level interpretability refers to scoring visits, and feature-level refers to ranking features present in visits according to their importance in predicting output. Fig. 4 shows the enhanced model architecture to achieve interpretability.

Fig. 4 LSTM Model Architecture with Interpretability. Proposed LSTM model architecture takes visit-level timestamp data (V_i) for each patient. This data passes through embedding layer and embedding weights for this layer are denoted by W_i where $I = \{1, 2, \dots, N\}$ N is the embedding layer dimension. The output of the embedding layer passes through LSTM layer to provide hidden state h_t . This hidden state passes through softmax layer to generate attention scores for each h_t as $a_{t1}, a_{t2}, \dots, a_{tN}$. We take average of values in $\{a_{t1}, a_{t2}, \dots, a_{tN}\}$ vector to obtain scalar attention values a_t for h_t . The scalar attention scores a_t are then used to take weighted sum of hidden state vectors h_t to obtain context vector c as $\{c_1, c_2, \dots, c_N\}$. A separate feed-forward network is used for demographic data to obtain $\{d_1, d_2, \dots, d_k\}$. Lastly, we concatenate vectors c and d and pass through dense layer to obtain the output.



4.3.1 Time-level interpretability

To enhance the interpretability at a time level, we added a softmax layer on top of the LSTM layers to compute the “attention score” for each timestep. In general, each LSTM unit generates a hidden output at each time step t , where $t = \{1, 2, \dots, T\}$. Hidden state h_t is computed by applying the non-linear transformation on input x_t to the LSTM unit at time t and hidden state of previous time step h_{t-1} (Eq. 1).

$$h_t \leftarrow LSTM(x_t, h_{t-1}) \quad (1)$$

where h_t is a vector of dimension N same as the dimension of the hidden layer of LSTM network. We calculated the attention score for each hidden state as shown in Eq. 2

$$a_{t1}, a_{t2}, \dots, a_{ti}, a_{ti+1}, \dots, a_{tN} = \text{softmax}(h_t) \quad (2)$$

where h_i is of dimension $|h_i| = N$ and N softmax scores are assigned to the h_i vector. To obtain scalar attention score value for each hidden state h_i we took an average of all the values in the vector $\{a_{t1}, a_{t2}, \dots, a_{ti}, a_{ti+1}, \dots, a_{tN}\}$ obtained in Eq. 2.

$$a_t = \left(\sum_{i=1}^N a_{ti} \right) \div N \quad (3)$$

The value a_i is calculated for each hidden state h_i . These scores are then used to compute the weighted sum of the hidden states (Eq. 4).

$$c = \sum_{t=1}^T a_t * h_t \quad (4)$$

where c is also a vector $\{c_1, c_2, \dots, c_i, c_{i+1}, \dots, c_N\}$ of N dimension, $|c| = N$ same as $|h_i| = N$. The vector c obtained is then used to predict future BMI. The scores computed using the softmax layer are used to visualize the visits that are given most importance by the LSTM layer.

4.3.2 Feature-level interpretability

To rank the input features in the multivariate time-series data, we added an embedding layer after the input layer and before the LSTM layer. We used weights from the embedding layer to compute the importance score for features in each timestep. Softmax scores for the timestep are multiplied (element-wise) with the embedding weight matrix for each input feature. Eq. 5 shows the s_i importance score calculation for i^{th} feature, where $b_i = a_{i1}, a_{i2}, \dots, a_{ij}, a_{ij+1}, \dots, a_{iN}$ is the softmax score output after the LSTM layer and W_i is weight matrix for the i^{th} feature from the embedding layer.

$$s_i = b_i \odot W_i \quad (5)$$

4.4 Transfer Learning

Transfer learning is used to enhance model performance by learning from a larger dataset. In our experiments, we created different sub-cohorts (48 in total) for different age ranges. While dividing our input data into sub-cohorts could improve its performance on learning specific age range patterns, this also meant reducing the input size of each of the models. This issue was especially more visible as the number of samples reduced gradually with increasing age ranges. Reduction in number of samples in pediatric datasets is common due to the higher rate of visits in earlier years of children’s life. To improve the performance of the model, we used the complete dataset for all age ranges. We initially created three models for predicting obesity at - 1 year in the future, 2 years in the future and 3 years in the future. After this, each of the three general models has been used as the basis for the 16 separate predictive models related to a similar prediction window.

4.5 Experiments

For training the LSTM models, we split data into 60:20:20 as training, validation and test data. Data split is performed such that the proportion of obese and non-obese samples is the same in the training and test data as in original data. Table 2 shows the number of obese and non-obese samples in each sub-cohort are shown in Table 2.

We used two LSTM layers for all models and Adadelta optimizer [30] with an initial learning rate of 0.05. Both L1 and L2 regularizations were used on the first LSTM layer. Two fully connected layers were used for the feed-forward network for static (demographic) data that didn’t need to go through the LSTM layers. We trained different models on different sub-cohorts based on different observation window and prediction age as explained in section 3.2. All models are trained on data in the observation window to predict the future BMI value in the respective prediction window. The predicted BMI values were then used to classify each sample into obese and non-obese classes.

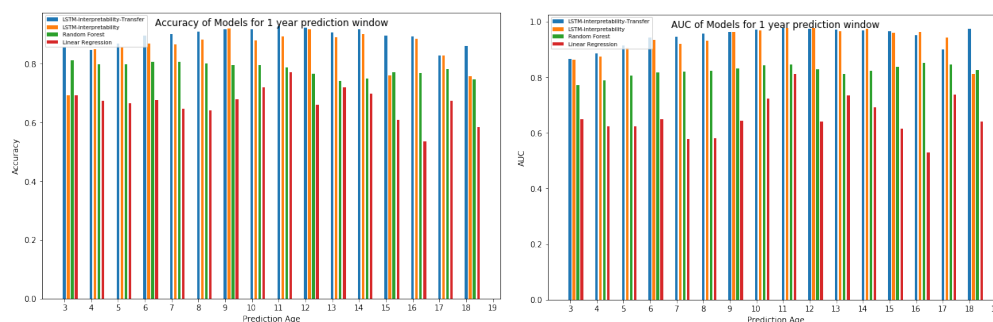
Table 2. Number of Obese and Non-obese Samples

Observation Window (Age year)	Prediction Age (Age year)	# of Obese Samples	# of Non-Obese Samples
0-2	3, 4, 5	5556, 7492, 8192	27842, 25906, 25206
1-3	4, 5, 6	7382, 8081, 8307	25464, 24765, 24539
2-4	5, 6, 7	6697, 6878, 7014	19977, 19796, 19660
3-5	6, 7, 8	5697, 5788, 6216	16227, 16136, 15708
4-6	7, 8, 9	4840, 5194, 5679	13492, 13138, 12653
5-7	8, 9, 10	4428, 4813, 5117	11182, 10797, 10493
6-8	9, 10, 11	4085, 4368, 4574	9032, 8749, 8543
7-9	10, 11, 12	3773, 3941, 4047	7542, 7374, 7268
8-10	11, 12, 13	3273, 3354, 3387	6118, 6037, 6004
9-11	12, 13, 14	2671, 2729, 2692	4933, 4875, 4912
10-12	13, 14, 15	2116, 2078, 2078	3718, 3756, 3756
11-13	14, 15, 16	1507, 1502, 1530	2688, 2693, 2665
12-14	15, 16, 17	1052, 1059, 1087	1766, 1759, 1731
13-15	16, 17, 18	651, 665, 690	1044, 1030, 1005
14-16	17, 18, 19	250, 249, 260	358, 359, 348
15-17	18, 19, 20	55, 57, 55	87, 85, 87

5 Results

We compared the performance of the baseline models, LSTM with interpretability as explained in section 4.3, and LSTM with interpretability trained on the larger dataset using transfer learning as explained in section 4.4. For the baseline models (linear regression and random forest regressor), we did 10-fold cross-validation and reported mean results over complete data. For LSTM models we did not use cross validations (due to heavy computing cost) and only report results on test data. Fig. 5 shows the Accuracy and AUC for all models separately based on prediction window size. Fig. 5 shows different plots for different prediction windows of 1 year, 2 years and 3 years. It compares performance of 1) Proposed LSTM model with interpretability trained using transfer learning, 2) Proposed LSTM model with interpretability trained without transfer learning, 3) Random Forest Regressor, 4) Linear Regression for each prediction window over different prediction windows separately. Fig. 6 analyzes the effect of the size of the prediction window in predicting obesity at certain prediction age. It compares the sensitivity, PPV, accuracy and AUC of the proposed LSTM model with interpretability trained using transfer learning. It shows how LSTM model perform for different prediction ages based on the size of the prediction window.

Fig. 5 Comparing Accuracy and AUC Results of 1) Proposed LSTM model with interpretability trained using transfer learning, 2) Proposed LSTM model with interpretability trained without transfer learning, 3) Random Forest Regressor, 4) Linear Regression. Separate results are shown for different prediction window – 1 year, 2 years and 3 years



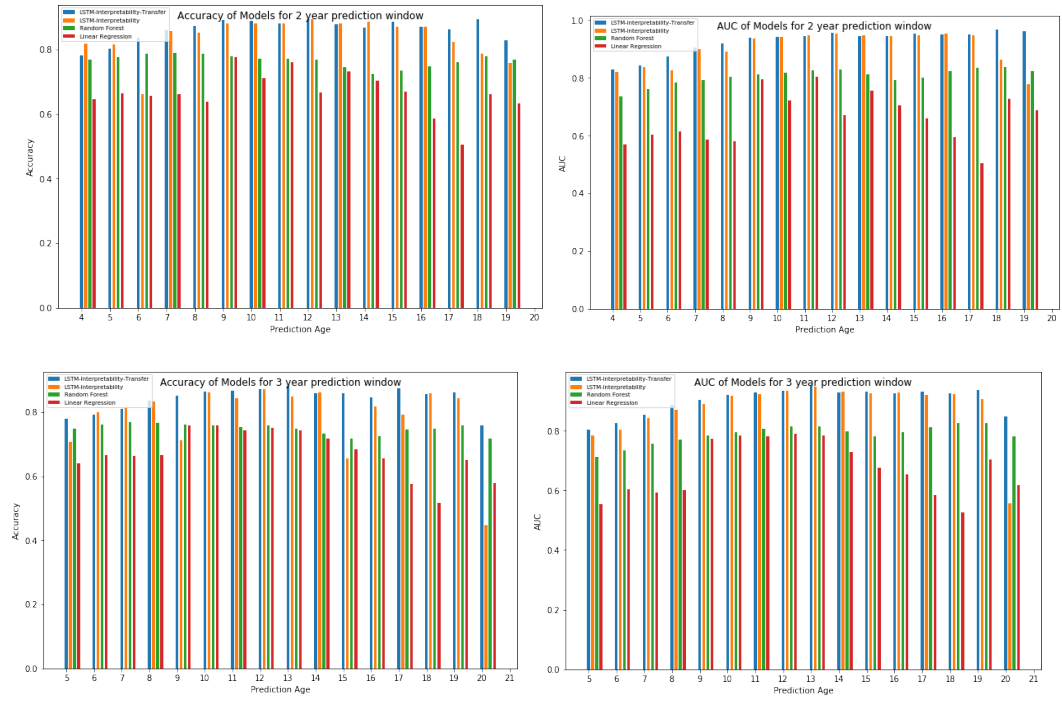
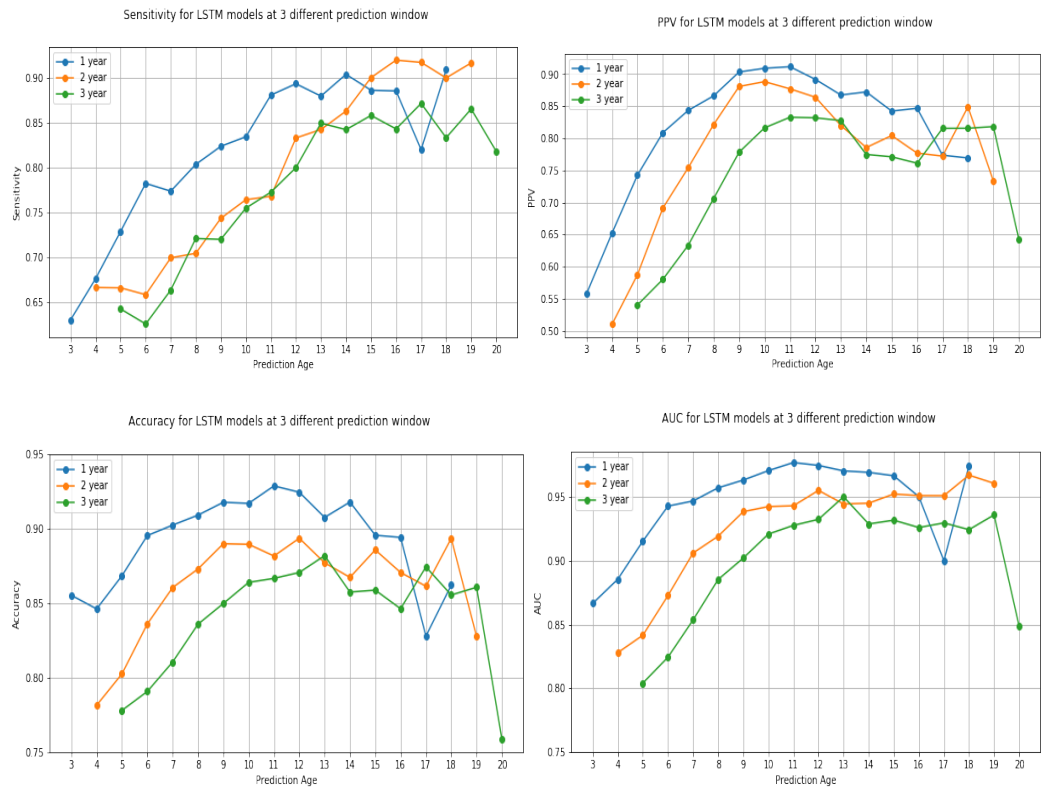


Fig. 6 Comparing the effect of the size of the prediction window in predicting obesity at a certain prediction age. Plots compare performance metrics - Sensitivity, PPV, Accuracy and AUC of LSTM with interpretability trained on transfer learning. Each plot compares the results obtained from different prediction windows for predicting obesity at a certain prediction age.



Additionally, feature importance is computed at both the individual and population level. Fig. 7 shows the ranking of the features in the top 3 important visits. This is feature importance for a sample individual patient. The values in each cell of Fig. 7 is the measurement value for corresponding feature. We also ranked feature importance at the population level by averaging feature importance for top 3 visits for all of the individual samples. Table 3 shows the top 20 most important features at the population level.

Fig. 7 Ranking of features for 3 most important timestamps. Gradient bar on right shows the importance score for each feature present in the 3 timestamps. For measurement medical variables each cell shows the value associated with it. If the feature is condition variable than the corresponding cell is blank and only represent the existence of that condition.

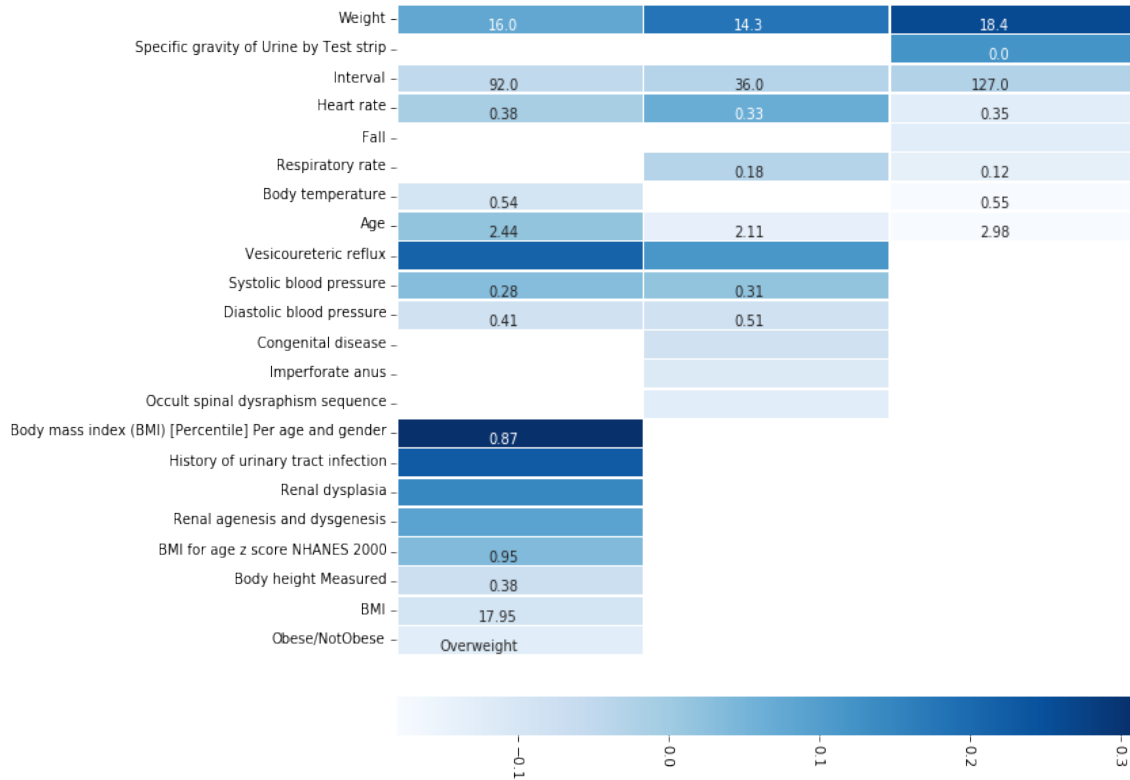


Table 3. Ranking of the features obtained after averaging the importance score of features obtained from all the samples in the test data.

Feature Ranking	Feature Description
1	BMI [Percentile] Per age and gender
2	Obese/Non-Obese Label
3	Allergic urticaria
4	Childhood obesity
5	Morbid obesity
6	Suspected clinical finding
7	Achondroplasia
8	MCH [Entitic mass] by Automated count
9	Cholesterol in LDL/Cholesterol in HDL
10	Hearing loss

11	Abnormal weight gain
12	Anomaly of chromosome pair 21
13	Erythrocytes [# /volume] in Body fluid
14	Obesity
15	Hyperactive behavior
16	Tachycardia
17	Requires respiratory syncytial virus
18	vaccination
19	CO2 1712
20	pH of Blood
	Hypoplastic left heart syndrome

6 Discussion

Our proposed model is applied to the obesity prediction in childhood and adolescence using EHR data. We employ an LSTM network and a separate feed-forward network to model dynamic (time-series) and static data in the EHR data. To transform these irregularly spaced and unequal number of clinical visits, we combined the visit data over a small fixed time window resulting in an equal number of time intervals. To use LSTM network on the EHR data we combined visits over the 30-day time-periods to obtain regularly spaced equal number of clinical visits for each patient. The width of the fixed time window is related to the stability of clinical events for the prediction task. We experimented with different window sizes of 6 months, 3 months, 30 days and 15 days. 30 days window size seemed to best capture the variations in clinical trajectories of patients for predicting obesity. As shown in Fig. 5, the performance of the LSTM is better than the two baseline models. i.e., linear regression and random forest. This shows that a recurrent neural network improves performance by taking into consideration the temporality of the data, a property that traditional methods do not have. Existing body of research shows that data temporality is important to capture weight gain trajectories and other medical history overtime [4]. However, random forest regressor shows higher performance for prediction at age of 20 using 3-year prediction window. This is due to the low number of samples in the corresponding sub-cohort and LSTM shows poor performance due to overfitting. But transfer learning helps improves performance for this sub-cohort by learning from samples of other sub-cohorts.

As shown in Fig. 5, the results obtained from LSTM model trained using transfer learning are higher as compared to LSTM trained on samples of specific sub-cohorts only. Transfer learning helps improve prediction performance especially for cohorts with a low number of samples. The results in Fig. 5 show that the performance of the last sub-cohort was significantly improved over the model trained on corresponding sub-cohorts only.

As it can be seen in Fig. 6, the closer the observation window is to the prediction time, the better the performance of the model. This means that prediction results obtained using 1 years prediction window are better than prediction results obtained using 2 years window which is better than prediction results obtained using 3 years prediction window. For both AUC and accuracy, all of the plots show a bell-shaped curve. In the beginning, the performance increases and then it starts to decrease after a certain prediction age. One reason for observing such pattern could be decreasing in number of samples and visits for that sub-cohort. There is a sharp decrease in performance for prediction at age of 20 years. For prediction at age of 20 years our model uses observation window of 15 to 17 years of age. Number of samples are very low for observation window of 15 to 17 years and prediction window of 20 years. The low number of samples in observation window of 15 to 17 years has more impact on 3 years prediction window as compared to 1 and 2 years of prediction window.

The performance obtained from our proposed model is comparable to performance in other cohort studies for obesity prediction. [8] [31] [18] [6]. Besides, superior predictive performance, we have also included interpretability capabilities to our proposed predictive model. We have ranked the features in each visit to provide insight into the prediction results. As shown in Fig. 7, we ranked the features for 3 most important visits. We picked the top 3 visits with highest attention weights and then ranked features for those visits. We ranked these features by calculating the importance score for features using Eq. 5. Here we can see that weight and BMI are most important features which is expected for predicting obesity. Among other highly ranked features, we can see that vesicoureteral reflux is given very high importance score. This condition is a type of kidney disease which is highly correlated to obesity in children [32]. In addition to the feature ranking for one sample shown in Fig. 7, we calculated the feature ranking over the complete dataset (with samples that are predicted obese) to get population level feature ranking. This shows the most important features in predicting obesity in children. As expected, BMI and previous and existing obesity level had the highest impact. Cholesterol and abnormal weight gain are also known to be correlated to obesity. Erythrocytes is related to kidney inflammation, which could also be a sign for future obesity. Tachycardia and heart rate are related to higher heart rate. Feature ranking also shows that hyperactive behavior is also an important factor in predicting future obesity, which coincides with the study in [33]. Our results collectively show that feature ranking obtained using the proposed LSTM model gives results that coincide with existing medical studies [34].

Our work can be extended in several ways. In future, we plan to add an additional attention layer after the initial dense layers processing static (demographic) data as well. Moreover, in this work, we fixed the observation windows to 2 years of data, in future, we can employ the proposed model with larger observation window size. Another future step would be expanding our transfer learning process by using data from other medical facilities.

7 Conclusion

In this study, we have developed a new deep neural network architecture for predicting future childhood obesity status in the next one, two, and three years. Specifically, we have used an LSTM-based for training our model using a longitudinal sample of patients' data obtained from a large US pediatric health system. An additional transfer learning process was used to improve the performance of the model developed for the sub-cohorts of the complete dataset. We showed that our LSTM-based model demonstrates a better performance as compared to traditional machine learning models that have been widely used in this important domain. For each individual sample, interpretability was achieved by ranking features in top three most important visits during the two years of training window. We have also calculated feature ranking for all samples in the data that were predicted obese in future. This gave us the list of features ranked according to their importance in predicting future obesity.

References

- [1] Centres for Disease Control and Prevention, "Childhood obesity facts," 24-Jun-2019. [Online]. Available: <https://www.cdc.gov/obesity/data/childhood.html>.
- [2] W. H. Dietz, "Health Consequences of Obesity in Youth: Childhood Predictors of Adult Disease," *Pediatrics*, vol. 101, no. Supplement 2, pp. 518–525, Mar. 1998.
- [3] S. Bleich, K. Vercammen, L. Zatz, J. Frelier, C. Ebbeling, and A. Peeters, "Interventions to prevent global childhood overweight and obesity: a systematic review," *Lancet Diabetes Endocrinol.*, vol. 6, January 10.
- [4] P. O. A. Monteiro and C. G. Victora, "Rapid growth in infancy and childhood and obesity in later life--a systematic review," *Obes. Rev. Off. J. Int. Assoc. Study Obes.*, vol. 6, no. 2, pp. 143–154, May 2005.

- [5] N. C. for H. S. Centres for Disease Control and Prevention, “Data Table of BMI-for-age Charts,” 23-Aug-2001. [Online]. Available: https://www.cdc.gov/growthcharts/html_charts/bmiagerev.htm.
- [6] N. Ziauddeen, P. J. Roderick, N. S. Macklon, and N. A. Alwan, “Predicting childhood overweight and obesity using maternal and early life risk factors: a systematic review,” *Obes. Rev.*, vol. 19, no. 3, pp. 302–312, 2018.
- [7] J. O. Robson, S. G. Verstraete, S. Shiboski, M. B. Heyman, and J. M. Wojcicki, “A risk score for childhood obesity in an urban Latino cohort,” *J. Pediatr.*, vol. 172, pp. 29–34, 2016.
- [8] R. Hammond *et al.*, “Correction: Predicting childhood obesity using electronic health records and publicly available data,” *PloS One*, vol. 14, no. 10, pp. e0223796–e0223796, 2019.
- [9] G. Bedogni, A. B. TsybakOv, and S. Berlin, “Clinical prediction models—a practical approach to development, validation and updating,” *development*, vol. 18, no. 500, pp. 53–99, 2009.
- [10] B. Shickel, P. J. Tighe, A. Bihorac, and P. Rashidi, “Deep EHR: a survey of recent advances in deep learning techniques for electronic health record (EHR) analysis,” *IEEE J. Biomed. Health Inform.*, vol. 22, no. 5, pp. 1589–1604, 2017.
- [11] J. Schmidhuber and S. Hochreiter, “Long short-term memory,” *Neural Comput.*, vol. 9, no. 8, pp. 1735–1780, 1997.
- [12] E. Choi, M. T. Bahadori, A. Schuetz, W. F. Stewart, and J. Sun, “Doctor ai: Predicting clinical events via recurrent neural networks,” 2016, pp. 301–318.
- [13] E. Choi, A. Schuetz, W. F. Stewart, and J. Sun, “Medical concept representation learning from electronic health records and its application on heart failure prediction,” *ArXiv Prepr. ArXiv160203686*, 2016.
- [14] E. Choi, A. Schuetz, W. F. Stewart, and J. Sun, “Using recurrent neural network models for early detection of heart failure onset,” *J. Am. Med. Inform. Assoc.*, vol. 24, no. 2, pp. 361–370, 2016.
- [15] T. Pham, T. Tran, D. Phung, and S. Venkatesh, “Deepcare: A deep dynamic memory model for predictive medicine,” 2016, pp. 30–41.
- [16] Z. Liang, G. Zhang, J. X. Huang, and Q. V. Hu, “Deep learning for healthcare decision making with EMRs,” 2014, pp. 556–559.
- [17] N. Wickramasinghe, “Deepr: a convolutional net for medical records,” 2017.
- [18] A. Morandi *et al.*, “Estimation of newborn risk for child or adolescent obesity: lessons from longitudinal birth cohorts,” *PloS One*, vol. 7, no. 11, p. e49919, 2012.
- [19] M. Steur *et al.*, “Predicting the risk of newborn children to become overweight later in childhood: the PIAMA birth cohort study,” *Int. J. Pediatr. Obes.*, vol. 6, no. sup3, pp. e170-178, 2011.
- [20] Y. Manios *et al.*, “Childhood Obesity Risk Evaluation based on perinatal factors and family sociodemographic characteristics: CORE index,” *Eur. J. Pediatr.*, vol. 172, no. 4, pp. 551–555, 2013.
- [21] C. Druet *et al.*, “Prediction of childhood obesity by infancy weight gain: an individual-level meta-analysis,” *Paediatr. Perinat. Epidemiol.*, vol. 26, no. 1, pp. 19–26, 2012.
- [22] Z. Pei *et al.*, “Early life risk factors of being overweight at 10 years of age: results of the German birth cohorts GINIplus and LISApplus,” *Eur. J. Clin. Nutr.*, vol. 67, no. 8,

p. 855, 2013.

- [23] D. Bahdanau, K. Cho, and Y. Bengio, “Neural machine translation by jointly learning to align and translate,” *ArXiv Prepr. ArXiv14090473*, 2014.
- [24] J. Zhang, K. Kowsari, J. H. Harrison, J. M. Lobo, and L. E. Barnes, “Patient2Vec: A Personalized Interpretable Deep Representation of the Longitudinal Electronic Health Record,” *IEEE Access*, vol. 6, pp. 65333–65346, 2018.
- [25] E. Choi, M. T. Bahadori, J. Sun, J. Kulas, A. Schuetz, and W. Stewart, “Retain: An interpretable predictive model for healthcare using reverse time attention mechanism,” 2016, pp. 3504–3512.
- [26] “PEDSnet: A pediatric Learning Health System,” *PEDSnet*. [Online]. Available: <http://pedsnet.org>. [Accessed: 01-Dec-2019].
- [27] “PEDSnet Common Data Model,” *PEDSnet*. [Online]. Available: <http://pedsnet.org>. [Accessed: 17-Dec-2019].
- [28] N. C. for H. S. Centres for Disease Control and Prevention, “Data Table of Infant Weight-for-age Charts,” 23-Aug-2001. [Online]. Available: https://www.cdc.gov/growthcharts/html_charts/wtageinf.htm.
- [29] J. Krause, A. Perer, and K. Ng, *Interacting with Predictions: Visual Inspection of Black-box Machine Learning Models*. 2016.
- [30] M. D. Zeiler, “ADADELTA: An Adaptive Learning Rate Method,” *ArXiv12125701 Cs*, Dec. 2012.
- [31] S. F. Weng, S. A. Redsell, D. Nathan, J. A. Swift, M. Yang, and C. Glazebrook, “Estimating Overweight Risk in Childhood From Predictors During Infancy,” *Pediatrics*, vol. 132, no. 2, pp. e414–e421, Aug. 2013.
- [32] “Vesicoureteral Reflux (VUR) | NIDDK,” *National Institute of Diabetes and Digestive and Kidney Diseases*. [Online]. Available: <https://www.niddk.nih.gov/health-information/urologic-diseases/hydronephrosis-newborns/vesicoureteral-reflux>. [Accessed: 01-Dec-2019].
- [33] E. A. Fliers *et al.*, “ADHD is a risk factor for overweight and obesity in children,” *J. Dev. Behav. Pediatr. JDBP*, vol. 34, no. 8, pp. 566–574, 2013.
- [34] K. Sahoo, B. Sahoo, A. K. Choudhury, N. Y. Sofi, R. Kumar, and A. S. Bhadoria, “Childhood obesity: causes and consequences,” *J. Fam. Med. Prim. Care*, vol. 4, no. 2, p. 187, Apr. 2015.